RSC Advances

PAPER

View Article Online
View Journal | View Issue

Cite this: *RSC Adv.*, 2025, **15**, 4000

A novel multifunctional fluorescent probe with ESIPT and AIE effects for the detection of Co^{2+} and HClO†

Chenxiang Lu,[a] Jiawei Xu,[a] Zhe Song,*[b] Guoqin Zhu*[c] and Zhenya Dai *[a]

Received 17th October 2024
Accepted 24th December 2024

DOI: 10.1039/d4ra07451c

rsc.li/rsc-advances

We developed a novel fluorescent probe featuring excited-state intramolecular proton transfer (ESIPT) and aggregation-induced emission (AIE) effects, which displayed dual-channel fluorescence emission. The probe detected both Co^{2+} and HClO with naked eye under daylight as well as through a fluorescence spectrophotometer. The probe exhibited a low detection limit for Co^{2+} at 2.823 μM, while the detection limit for HClO was 11.55 μM. When the probe (10 μM) was mixed with Co^{2+}, the fluorescence intensity at 556 nm rapidly decreased within 10 minutes and stabilized after 40 minutes, while for HClO, it took 960 min to observe the same decrease in intensity within 960 min. The probe (10 μM) achieved naked-eye detection of Co^{2+} recognition under daylight; however, achieving naked-eye detection of HClO under daylight necessitated higher concentrations (500 μM). Thus, this probe shows promising potential for environmental monitoring and water quality detection.

1. Introduction

HClO is prevalent in food preservation and sanitation practices, serving as a potent oxidizing agent, and effective in neutralizing harmful microorganisms, including bacteria. For living organisms, HClO is a dual-edged tool. It is indispensable in the fight against invading pathogens[1] and the maintenance of redox balance.[2–4] However, excessive HClO could become hazardous when reacted with biological macromolecules, such as proteins, DNA, RNA, amino acids, and cholesterol.[5,6] These reactions could lead to oxidative stress, Alzheimer's disease,[7,8] cardiovascular disease,[9,10] inflammatory bowel disease,[11] and organ transplant rejection.[12]

Co^{2+} is naturally present in the Earth's crust, water bodies, flora, and fauna, and is ubiquitous within essential organs, such as the liver, bones, and kidneys, where it participates in complex signaling processes.[13] Furthermore, Co^{2+} serves as a vital component of vitamin B_{12} and other cobalamins, playing crucial roles in iron metabolism and the synthesis of hemoglobin.[14,15] However, both excessive accumulation and deficiency of Co^{2+} could lead to adverse health outcomes, including growth retardation, anemia, decreased appetite, reduced lactation,[16] cardiovascular diseases,[17–19] and pulmonary damage.[20,21]

Therefore, there is an urgent need to develop reliable methods to monitor HClO and Co^{2+} concentrations. Unlike traditional analytical techniques, such as electroanalysis, potentiometry, chemiluminescence, bioanalytical methods and chromatography,[22–28] fluorescence probes offer several advantages, including high selectivity and sensitivity, rapid response rates, and the capability for real-time detection.[29–36]

Fluorescent probes designed for Co^{2+} commonly engage in chelation reactions, resulting in alterations to the probe's fluorescent characteristics. This chelation might lead to a decrease in the fluorescence intensity. However, in certain cases, that could trigger chelation-enhanced fluorescence (CHEF) or aggregation-induced emission enhancement (AIEE), resulting in an enhancement of fluorescence intensity. For instance, probe 1, which was designed by Ghazali *et al.*,[37] complexed with Co^{2+} at a chelation ratio of 2 : 3. In the presence of Co^{2+}, CHEF was activated, which increased the molecular rigidity and subsequently intensified the fluorescence intensity. In contrast, in probe 2, which was developed by Kim *et al.*,[38] the fluorescence emission underwent a redshift following chelation with Co^{2+} (Fig. 1). The design strategy for HClO probes primarily involve a set of unique reaction, resulting in a change in the probe's fluorescence intensity. As shown in Fig. 2, leveraging the oxidizing nature of HClO, Shi *et al.*[39] exploited the reductive properties of sulfur atoms to design a fluorescent probe for the detection of HClO, designated as Probe 3. The principle behind the probe 4 synthesized by Xia *et al.*[40] for the recognition of HClO was similar to that of probe 3. Fluorescent probes designed based on the oxidizing nature of HClO are prone to

[a]*Department of Medicinal Chemistry, School of Pharmacy, China Pharmaceutical University, 24 Tongjiaxiang, Nanjing, 210009, P. R. China*

[b]*China Pharmaceutical University Center for Analysis and Testing, 24 Tongjiaxiang, 210009, P. R. China. E-mail: daizhenya@hotmail.com*

[c]*Department of Geriatric Gastroenterology, Jiangsu Province Hospital, The First Affiliated Hospital of Nanjing Medical University, Nanjing Medical University, 300 Guangzhou Road, Nanjing, 210029, P. R. China*

† Electronic supplementary information (ESI) available. See DOI: https://doi.org/10.1039/d4ra07451c

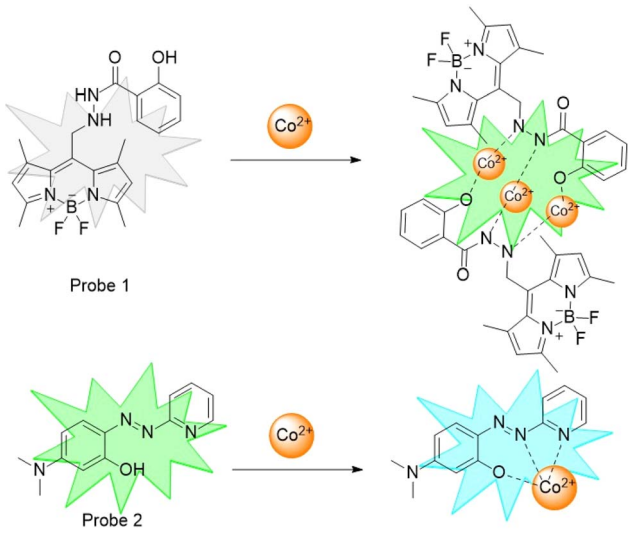

Fig. 1 Probes that chelate with Co^{2+}.

interference in complex environments, while those relying on specific reactions for HClO recognition demonstrate enhanced specificity and interference resistance. As shown in Fig. 3, Zhu *et al.*[41] utilized rhodamine as the fluorophore. In the presence of HClO, the 1,3,4-oxadiazole ring opened, which triggered the probe fluorescence emission. Xu *et al.*[42] introduced an electron-deficient carbon–carbon double bond into probe 6, which reacted with HClO under mild conditions, causing the double bond to break. Yang *et al.*[43] designed a Schiff base probe 7 that decomposed in the presence of HClO, leading to a change in the fluorescence peak and thus achieving the detection of HClO. Chen *et al.*[44] synthesized probe 8 with diaminomalononitrile as the recognition site, which hydrolyzed in the presence of HClO to activate fluorescence. Wu *et al.*[45] reported that *N*,*N*-dimethylthioformamide reacted with HClO, leading to its removal and exposure of the phenolic hydroxyl group. This activation of the ESIPT effect resulted in strong fluorescence emission.

In the 1950s, Weller *et al.*[46] first highlighted the benefits of the ESIPT (Excited-State Intramolecular Proton Transfer) effect, such as dual-channel fluorescence emission and large Stokes shifts, attracting significant interest. The ESIPT effect involved proton transfer from a donor (*e.g.*, amino or hydroxyl groups) to an acceptor (*e.g.*, nitrogen or oxygen atoms), exemplified by keto–enol tautomerism. This process followed a four-level cycle: a fluorescent molecule absorbs energy and transitions from the ground state (E) to the excited state (E*). Some excited molecules (E*) released enol fluorescence and returned to the ground state (E), while others transferred a proton to form a keto structure (K*), released keto fluorescence, fell back to the ground state (K), and then reverted to the enol form (E) *via* reverse proton transfer (RPT)[47–50] (Fig. 6). ESIPT probes are highly valued in fields such as fluorescence,[51] bioimaging,[52,53] and luminescent materials[54,55] due to their dual-channel emission, large Stokes shift, and extended fluorescence lifetime. However, their sensitivity to solvent microenvironments, especially protic solvents, severely constrains their practical utility.[56] In 2001, Tang Benzhong's group first reported the AIE (Aggregation-Induced Emission) effect.[57] AIE fluorescent molecules were non-emissive in the solution but emitted strong fluorescence when aggregated or in the solid state, offering a new platform for developing fluorescent probes.

The emergence of the AIE effect has provided new avenues for the development of ESIPT effects. Fluorescent probes, benefiting from the synergistic interplay of ESIPT and AIE effects, not only inherited the fluorescence advantages of these effects but also mutually enhanced each other, thereby improving the fluorescence performance of the probes. The AIE and ESIPT effects endowed probes with various advantages; for instance, large Stokes shifts could prevent self-absorption phenomena, multi-channel fluorescence emission could provide greater flexibility and operability for practical probe applications, and the ability for aggregate fluorescence emission could minimize the solvent's impact.

2. Experimental section

2.1 Materials and instrumentation

All chemicals were purchased directly through commercial channels and used without further purification. The specific product information sources are shown in the ESI.† The

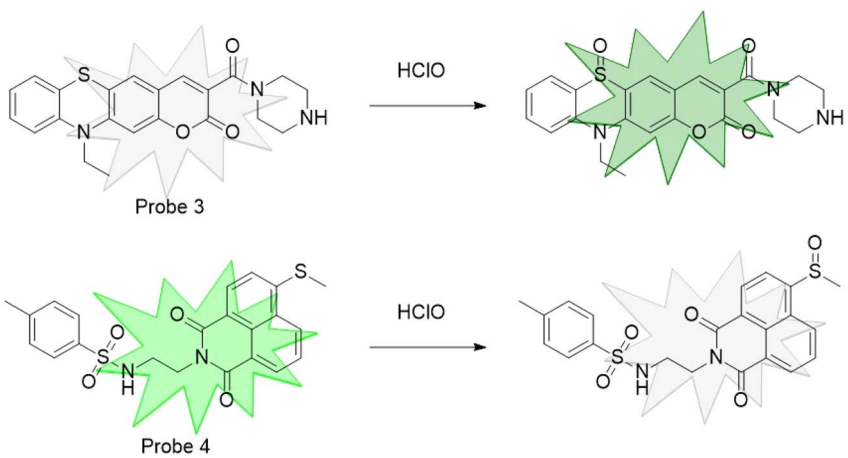

Fig. 2 Probes that utilize the oxidizing property of hypochlorous acid for its detection.

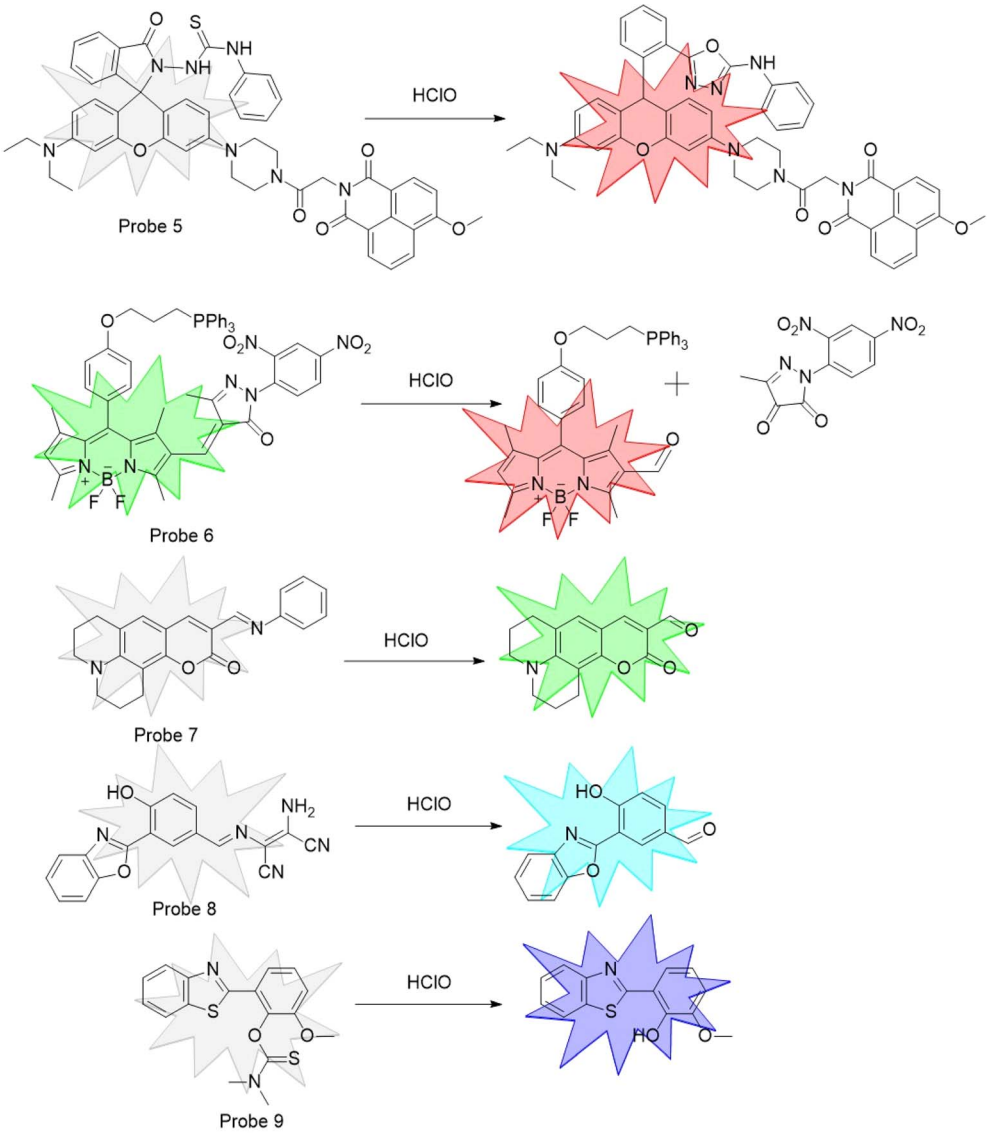

Fig. 3 Probes that recognize hypochlorous acid through specific reactions.

instruments used in the experiment included a spectrophotometer, ESI-MS, nuclear magnetic resonance (NMR) and Malvern Zetasizer. The details about the manufacturer and model of the instrument are shown in the ESI.†

2.2 General procedure for analysis

The synthesis of the probe is shown in Fig. 4. Benzophenone and 4-hydroxybenzophenone were combined to form the TPE core through a McMurry coupling reaction. Subsequently, aldehyde groups were introduced at the *ortho* position of the phenolic hydroxyl through a Duff reaction, which was combined with 2-hydrazinobenzimidazole to construct the recognition site for HClO, thus completing the synthesis of the probe. The probe was rich in heteroatoms, endowing it with the ability to chelate metal ions.

2.2.1 Synthesis of compound AE-1. Under a nitrogen atmosphere and ice bath, zinc powder (7 g, 107.69 mmol, 4 eq.) was scattered in anhydrous tetrahydrofuran (THF) (60 mL). Titanium tetrachloride (6 mL, 54.59 mmol, 2 eq.) was then added dropwise to the reaction system, resulting in a gray turbid mixture. The mixture was kept in the ice bath for 30 min. Then, the reaction mixture was stirred for 30 minutes at 70 °C. Subsequently, dibenzyl ketone (5 g, 27.44 mmol, 1 eq.) and 4-hydroxydibenzyl ketone (5.44 g, 27.44 mmol, 1 eq.) were dissolved in 20 mL of anhydrous THF and added dropwise to the reaction mixture, which was then refluxed at 70 °C for 14 hours. After completion of the reaction, the solvent was removed under reduced pressure. The residue was quenched with saturated sodium bicarbonate solution, followed by extraction with diethyl ether. The organic phases were then combined and evaporated under reduced pressure. The crude product was purified by column chromatography on silica gel, affording a yellow solid AE-1 (4.3 g, 45% yield). ^{1}H NMR (300 MHz, DMSO) δ 9.35 (s, 1H), 7.46–7.34 (m, 1H), 7.14–7.03 (m, 8H), 6.99–6.92

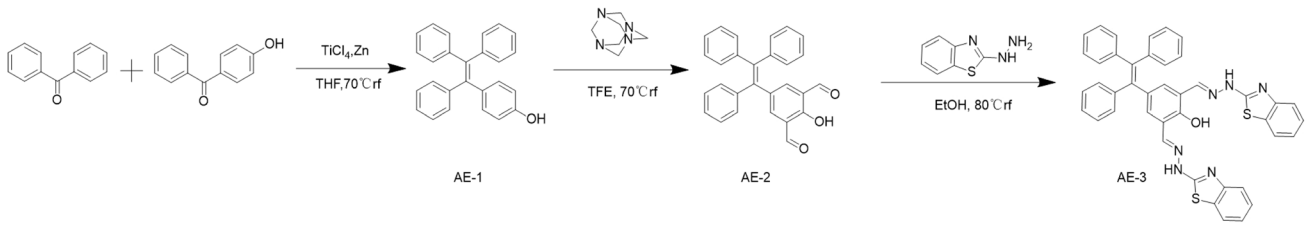

Fig. 4 Synthesis process for the compound AE-3.

(m, 6H), 6.78–6.70 (m, 2H), 6.50 (d, $J = 8.5$ Hz, 2H). ESI-m: $m/z =$ 347.14 $[M]^-$.

2.2.2 Synthesis of compound AE-2. A mixture of AE-1 (3 g, 8.62 mmol, 1 eq.) and scopolamine (6.03 g, 43.01 mmol, 5 eq.) was dissolved in 50 mL of trifluoroacetic acid (TFA). The mixture was heated at 70 °C for 4 hours. After completion of the reaction, 50 mL of ice water was added, followed by the addition of sodium bicarbonate to adjust the pH to neutral. The mixture was then extracted with EA and the organic phases were combined and evaporated under reduced pressure. The crude product was purified by column chromatography on silica gel, affording a yellow solid AE-2 (1.78 g, 51.13% yield). ^{1}H NMR (300 MHz, DMSO) δ 10.75 (s, 1H), 10.11 (s, 1H), 9.88 (d, $J =$ 4.5 Hz, 1H), 7.67 (dd, $J = 8.1$, 6.1 Hz, 2H), 7.16 (dddd, $J = 21.6$, 14.3, 8.3, 2.5 Hz, 10H), 7.05–6.93 (m, 4H), 6.76 (dd, $J =$ 8.6, 3.1 Hz, 1H). ESI-m: $m/z = 403.13$ $[M]^-$.

2.2.3 Synthesis of compound AE-3. The mixture of AE-2 (200 mg, 0.495 mmol, 1 eq.) and 2-hydrazinobenzothiazole (189 mg, 1.144 mmol, 2.3 eq.) was dissolved in 3 mL of ethanol. The reaction mixture was refluxed at 80 °C for 22 hours. After completion of the reaction, the mixture was filtered, and the filter cake was rinsed with ethanol and afforded yellow-green solid AE-3 (197 mg, 57.02% yield). ^{1}H NMR (300 MHz, DMSO) δ 12.17 (s, 2H), 8.25 (s, 1H), 8.06 (d, $J = 5.7$ Hz, 1H), 7.76 (d, $J =$ 7.7 Hz, 2H), 7.47 (q, $J = 7.2$, 6.1 Hz, 3H), 7.29 (t, $J = 3.7$ Hz, 3H), 7.12 (dq, $J = 34.5$, 8.7, 8.0 Hz, 16H), 6.85 (dd, $J = 8.5$, 2.3 Hz, 1H), 6.71 (d, $J =$ 8.4 Hz, 1H). ^{13}C NMR (75 MHz, DMSO) δ 167.07, 166.49, 155.44, 144.79, 143.18, 143.04, 140.62, 139.48, 134.32, 133.44, 132.31, 131.28, 130.79, 127.98, 126.83, 126.62, 126.01, 121.87, 121.57, 119.05, 115.72. ESI-m: $m/z = 697.18$ $[M]^-$.

2.3 Optical studies

2.3.1 General process. A stock solution of probe 1 (100 μM) was prepared in the reagent THF. A phosphate buffer solution was prepared in pure water. A stock solution of the metal ions (100 μM) including Fe^{3+}, Al^{3+}, Cd^{2+}, Mg^{2+}, Cu^{2+}, Co^{2+}, Ba^{2+}, Mn^{2+}, Ca^{2+}, Cr^{3+}, Ni^{2+}, Zn^{2+} and Fe^{2+} were prepared in phosphate buffer solution. A stock solution of other analytes (1 mM) including SCN^-, NO_2^-, NO_3^-, SO_4^{2-}, SO_3^{2-}, HClO, Cl^-, CH_3COO^- and H_2O_2 was prepared in the phosphate buffer solution. For a typical optical study, a solution containing probe 1 (10 μM) in THF/phosphate buffer solution was prepared. Then, 3.0 mL of that solution was placed in a quartz cuvette. After the addition of the analyte of interest (the total volume change of the solution in the cuvette was less than 2%), the fluorescent spectra were recorded. Fluorescence spectroscopy analysis, unless otherwise stated, was operated at $\lambda_{ex} = 360$ nm. The detailed operation steps are shown in the ESI.†

2.3.2 The calculation for the limit of detection (LOD) and Benesi–Hildebrand association constant (K_a). The limit of detection (LOD) of probe to target analyte was calculated by the formula:

$$\mathrm{LOD} = 3\sigma/k$$

where σ (standard deviation) was the standard deviation of the detection signal of the blank sample of the fluorescence probe tested several times; k is the slope of the linear relationship between the detection signal of the fluorescence probe and the concentration of the target analyte. For Co^{2+} and HClO, we used the fluorescence intensity ($F = 556$ nm) as the detection signal.

The determination of the association constant was accomplished by employing the canonical Benesi–Hildebrand method.

$$1/(F - F_{\min}) = 1/K_a(F_{\max} - F_{\min})/[\mathrm{M}] + 1/(F_{\max} - F_{\min})$$

F represents the fluorescence intensity of the probe in the presence of varying concentrations of the target analyte. $F_{\min}$ denoted the fluorescence intensity of the probe in the absence of any interfering substances. $F_{\max}$ signified the fluorescence intensity when the probe reached equilibrium with the target analyte through chelation. M represents the concentration of the target analyte. K_a is the association constant.

3. Results and discussion

3.1 Design and synthesis

To design a novel AIE and ESIPT probe for the detection of HClO and Co^{2+}, we used TPE units to afford the AIE effect, the proton transfer of 2-(2-benzothiazolyl) hydrazone and phenol hydroxyl to provide ESIPT effect.

The electron-rich groups of the Schiff base and phenolic hydroxyl group have the potential to chelate with metal ions. Attaching two Schiff base units adjacent to the phenolic hydroxyl group enhanced the formation of a stable multidentate chelation structure with metal ions. On one hand, the probe detected by chelating metal ions with Schiff base structures or even phenolic hydroxyl groups, quenching keto-form fluorescence and even enol-form fluorescence. On the other hand, 2-(2-benzothiazolyl) hydrazone is a classic recognition site for detecting HClO.[58] In the presence of HClO, the

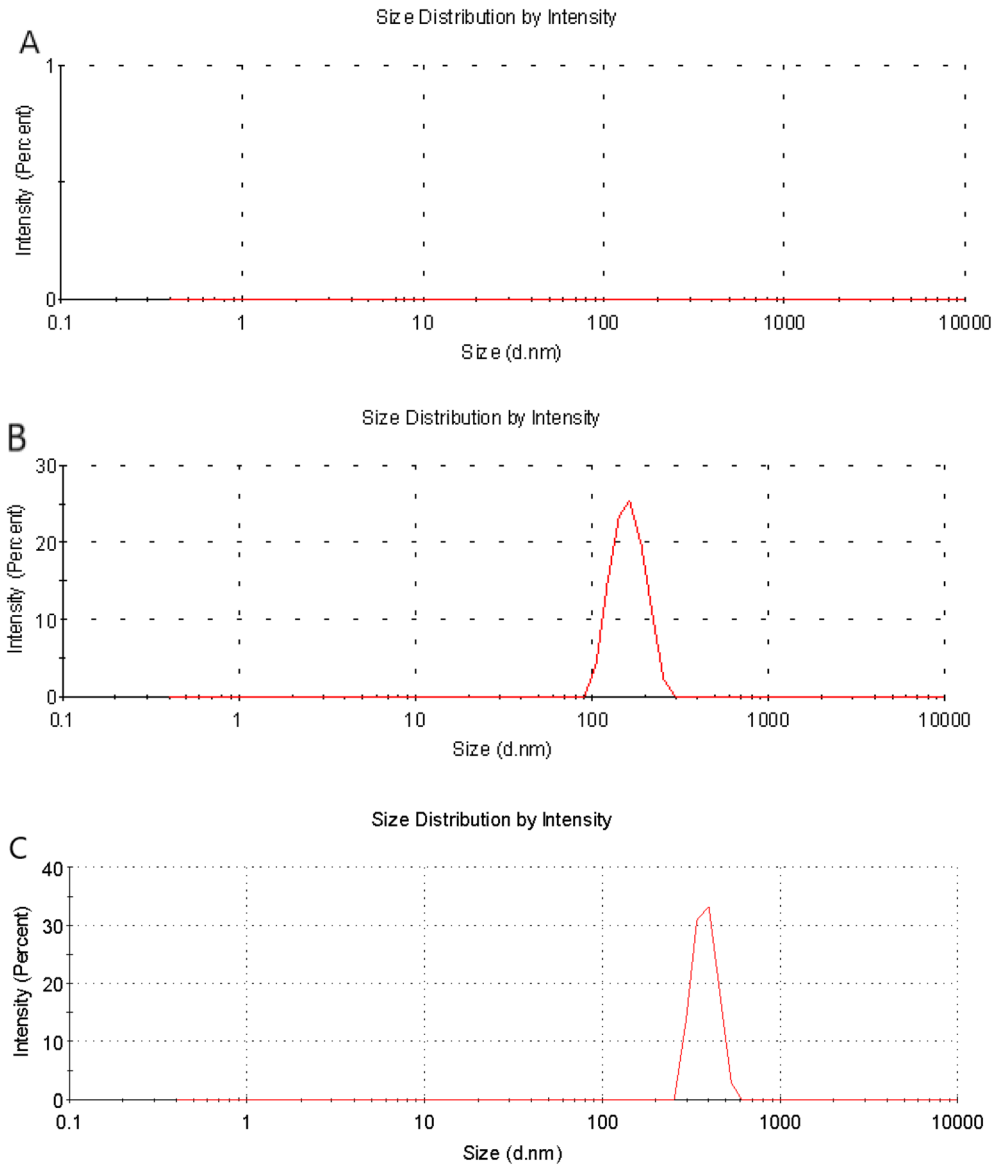

Fig. 5 Dynamic light scattering (DLS) study of probe AE-3 (10 μM) with different percentages of H_2O: (A) 0%, (B) 50%, (C) 90%.

hydrazone and benzothiazole ring cyclized to form a triazole. This particular reaction was used to detect HClO, as it converted the 2-(2-benzothiazolyl) hydrazone into triazole, quenching keto-form fluorescence or altering enol-form fluorescence.

3.2 AIE and ESIPT effect

With AE-3 in hand, we discovered that it exhibited two-channel emission (Fig. 6) through fluorescence spectroscopy analyses, showing a typical ESIPT phenomenon. To demonstrate the AIE effect of AE-3, we incubated it in THF solutions with water content ranging from 0% to 99%. As shown in Fig. 7, the probe exhibited fluorescence emission peaks at 474 nm and 556 nm, corresponding to the enol-form and keto-form fluorescence, respectively. When the water content in the solvent increased from 60% to 95%, the intensity of the two emission peaks was significantly enhanced (Fig. S1–S2†).

Upon meticulous analysis of the UV absorption spectra of the probe in the solution with varying water contents, we observed significant spectral alterations (Fig. S3†). Specifically, within the range of 10% to 70% water content, the probe exhibited distinct UV absorption peaks at 231 nm and 252 nm, which might be attributed to the benzothiazole. Additionally, the absorption peak at 370 nm corresponded to the π–π* transitions of the large conjugated benzene rings. As the water content increased, the polarity of the solvent heightened, leading to a redshift of the π–π* transition peaks of the benzene ring and the σ–π* transition peaks of benzothiazole displayed a blueshift. With further enhancement of the water content, the aggregation of the probe intensified, reducing the actual concentration of the probe dissolved in the solution, which ultimately led to a notable decrease in absorbance. Meanwhile, the probe features Schiff base structures and large conjugated benzene

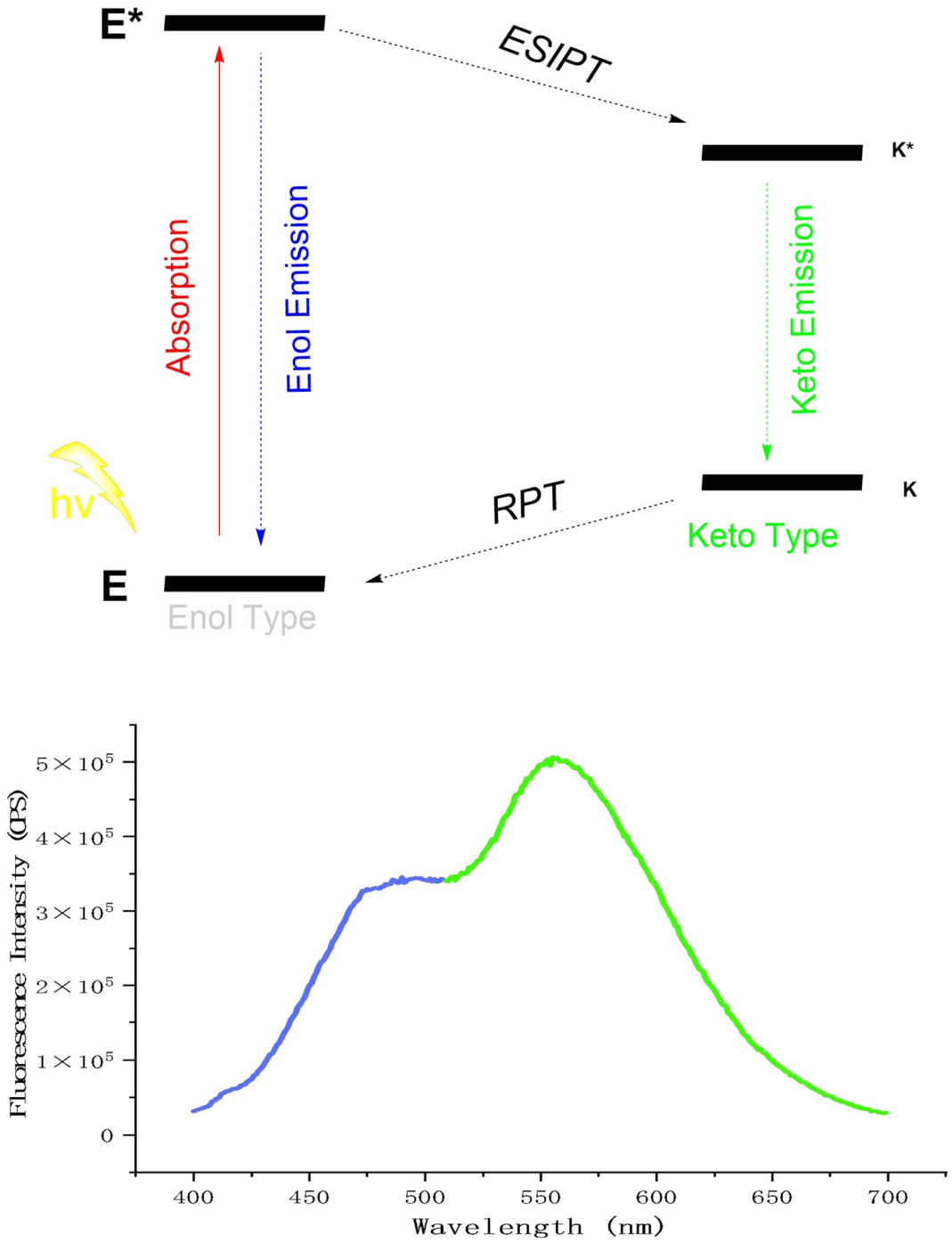

Fig. 6 AIE and ESIPT effects of AE-3.

rings, which contributed to the poor solubility of the probe. These changes in the UV spectra also, to some extent, demonstrated the aggregation characteristics of the probe in different solvents.

In our investigation of the aggregation behavior of probes in the solution with varying water content using dynamic light scattering (DLS), we observed the following: when the solution contained 10% water, no significant particles were detected, indicating that the probe was completely dissolved in THF/H_2O (9 : 1). Upon increasing the solution water content to 50%, DLS measurements revealed that the average size of the aggregated probe was 159.5 nm, indicating a certain degree of probe aggregation. Elevating the aqueous fraction of the solution to 90% led to a significant enlargement of the aggregate dimensions, with the average size reaching 873.9 nm (Fig. 5). This phenomenon indicated that as the water content in the solvent increased, the probe gradually underwent aggregation.

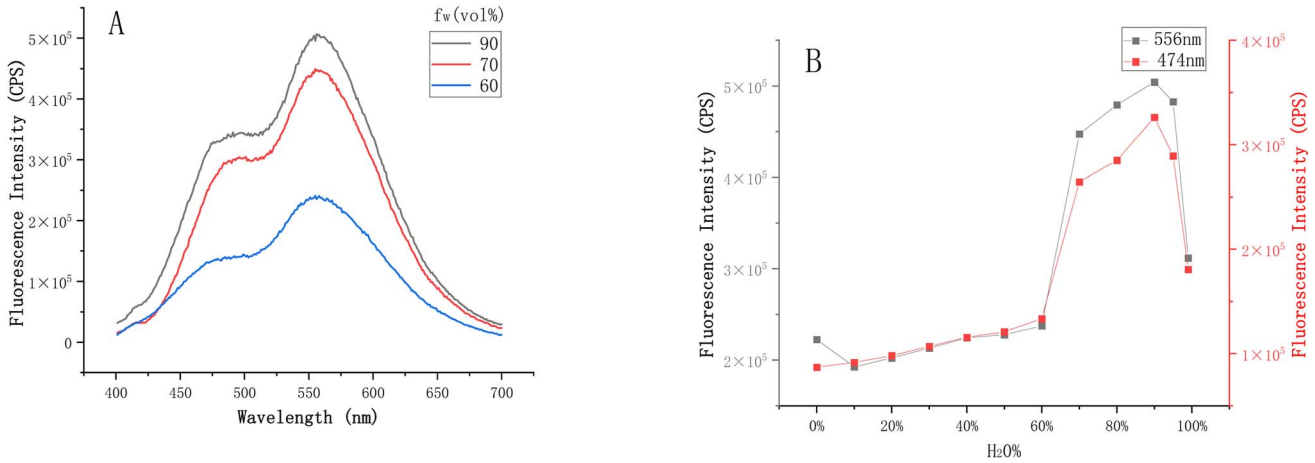

Fig. 7 (A) Fluorescence spectra of AE-3 (10 μM) in a THF/phosphate buffer (50 mM, pH = 7.4) with water contents of 60%, 70% and 90%. (B) Fluorescence intensity of AE-3 (10 μM) at 556 nm and 474 nm with the water content ranging from 0% to 99%.

3.3 Fluorescence response of AE-3 to Co^{2+}

The initial phase of our study involved conducting selective fluorescence assays on AE-3 (10 μM) in the presence of various metal ions: Fe^{3+}, Al^{3+}, Cd^{3+}, Mg^{2+}, Cu^{2+}, Co^{2+}, Ba^{2+}, Ca^{2+}, Cr^{3+}, Mn^{2+}, Ni^{2+}, Zn^{2+} and Fe^{2+} each at a concentration of 10 μM. Upon the addition of the above-mentioned metal ions to the AE-3 solution, the fluorescence spectrum remained largely unaffected, with the exception of notable changes observed with Co^{2+} and Cu^{2+} (Fig. S4†). The paramagnetic nature of Cu^{2+} resulted in quenching of the fluorescence peaks at 474 nm and 556 nm (Fig. 8). Subsequently, the probe's anti-interference ability during Co^{2+} recognition was evaluated (Fig. 8 and S5†).

The limit of detection (LOD) for Co^{2+} was determined by the slope of the fluorescence intensity at F556 nm from continuous titration experiments with different equivalents of Co^{2+} and the standard deviation of 10 blank samples of AE-3 (10 μM). The absolute slope of the linear relationship between the fluorescence intensity at F556 nm and Co^{2+} (0.1–0.9 eq.) was found to be 31 716.07 (Fig. S6†). Additionally, the standard deviation of the fluorescence intensity at F556 nm for the 10 blank samples was calculated as 29 846.30 (Fig. S7†). The calculated limit of detection (LOD) using the formula $3\sigma/k$ was 2.823 μM.

To investigate the binding mode of the probe and Co^{2+}, the Job's plot curve method was employed. As shown in Fig. 9, when the total concentration of the probe and Co^{2+} was kept constant, the fluorescence intensity gradually decreased with an increase in the proportion of Co^{2+}. When the concentration ratio of Co^{2+} to the total concentration exceeded 0.5, the fluorescence intensity tended to stabilize, indicating a 1 : 1 binding ratio between the probe and Co^{2+}. By employing the Benesi–Hildebrand method, a linear regression equation was established, where F_{max} denotes the fluorescence intensity of the probe at a 1 : 1 concentration ratio with Co^{2+}. The calculated association constant (K_a) was determined to be 475 579.02.

To evaluate the sensitivity and stability of the probe in detecting Co^{2+} ions, we conducted fluorescence spectroscopy analysis at various incubation durations (Fig. 10). The

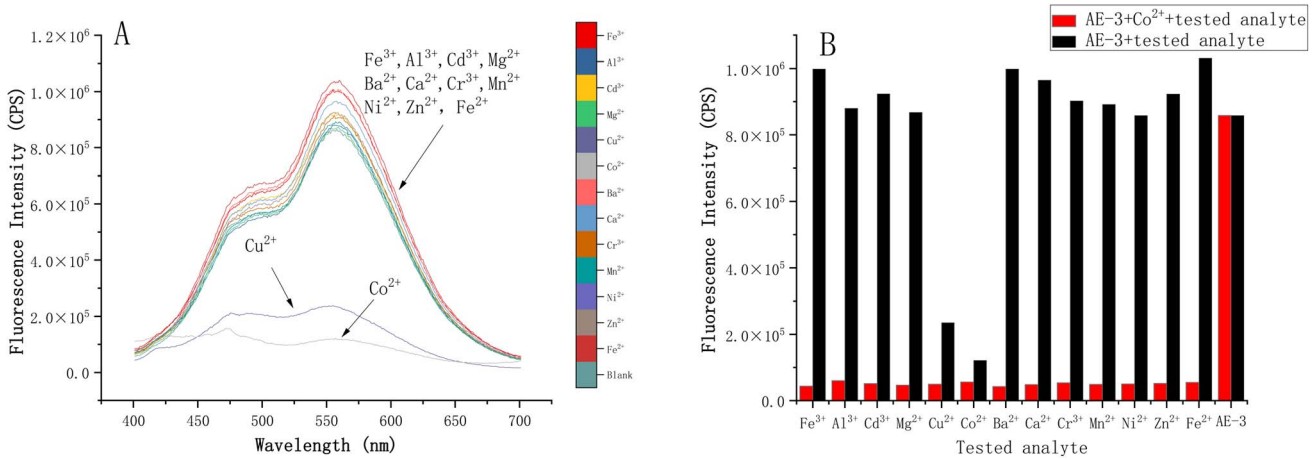

Fig. 8 (A) Fluorescence spectra of AE-3 (10 μM) in a THF/phosphate buffer (1/9, v/v, 50 mM, pH = 7.4) in the presence of Fe^{3+}, Al^{3+}, Cd^{3+}, Mg^{2+}, Cu^{2+}, Co^{2+}, Ba^{2+}, Ca^{2+}, Cr^{3+}, Mn^{2+}, Ni^{2+}, Zn^{2+}, and Fe^{2+}. (B) Fluorescence intensity of AE-3 (10 μM) at 556 nm.

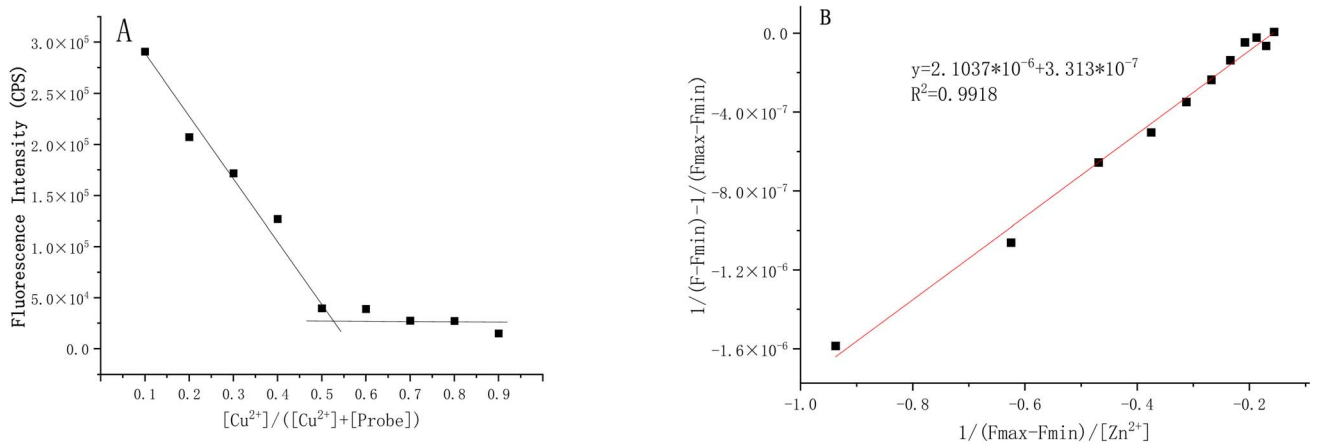

Fig. 9 (A) Job's plot. (B) Linear regression equation of Benesi–Hildebrand.

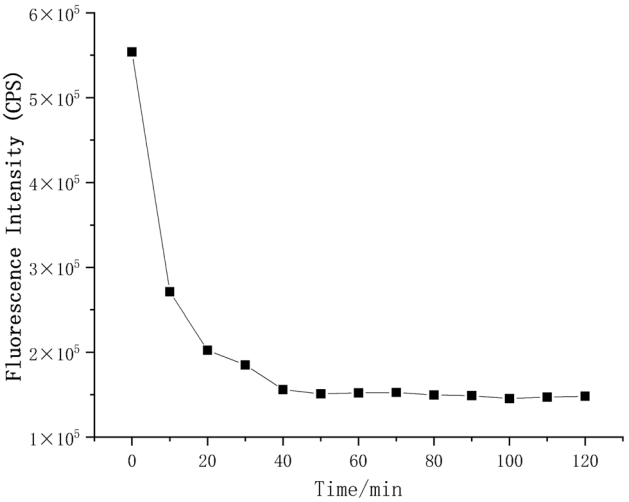

Fig. 10 Point-line plot of the fluorescence intensity at 556 nm *versus* incubation time of the AE-3 (10 μM) with Co^{2+}.

fluorescence intensity of AE-3 at 556 nm exhibited a rapid decline within the first 10 minutes, followed by a gradual leveling off, and stabilization after 40 minutes.

3.4 Fluorescence response of AE-3 to HClO

Similarly, we first conducted selective tests on AE-3 (10 μM) using SCN^-, NO_2^-, NO_3^-, SO_4^{2-}, SO_3^{2-}, Cl^-, CH_3COO^-, H_2O_2 and HClO (50 μM). Upon the addition of HClO, the fluorescence intensities at 474 nm and 556 nm both decreased, while a new peak emerged at 594 nm. There were no significant changes in the fluorescence spectra upon the addition of other analytes (Fig. 11 and S8†). Then, the anti-interference ability of AE-3 recognition was evaluated (Fig. S9–S10†). AE-3 (10 μM) demonstrated robust anti-interference capacity in HClO detection and exhibited exceptional selectivity and anti-interference ability for HClO detection.

The absolute slope of the linear relationship between the fluorescence intensity at 556 nm of AE-3 (10 μM) and HClO (0–6 eq.), measured by the continuous titration method, was found

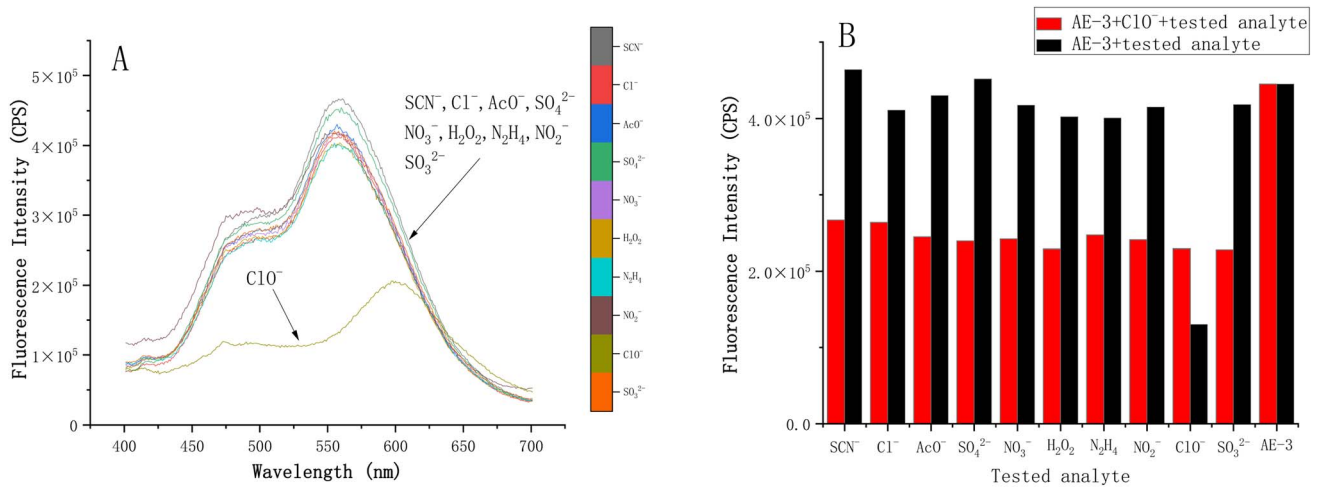

Fig. 11 (A) Fluorescence spectra of AE-3 (10 μM) in a THF/phosphate buffer (1/9, v/v, 50 mM, pH = 7.4) in the presence of SCN^-, Cl^-, CH_3COO^-, SO_4^{2-}, NO_3^-, H_2O_2, NO^{2-}, ClO^- and SO_3^{2-}. (B) Fluorescence intensity of AE-3 (10 μM) at 556 nm.

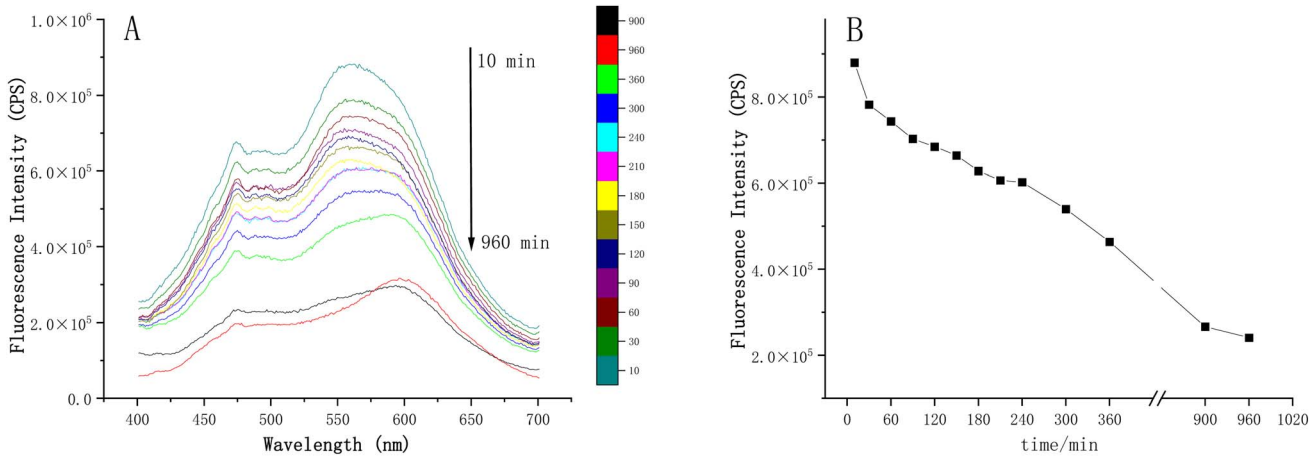

Fig. 12 (A) Fluorescence spectra of AE-3 (10 μM) and HClO (50 μM) incubated for different times (10 min–960 min). (B) Fluorescence intensity at 556 nm *versus* the incubation time of the AE-3 (10 μM) with HClO.

to be 7755.17 (Fig. S11†). The standard deviation of fluorescence intensity at 556 nm for the 10 blank specimens was calculated as 29 846.30 (Fig. S7†). The calculated limit of detection (LOD) using the formula $3\sigma/k$ was 11.55 μM.

Similarly, to assess the sensitivity and stability of the probe in HClO recognition, fluorescence spectroscopy analysis was conducted at different incubation times (Fig. 12). We noted a gradual decrease in the fluorescence intensity at 556 nm of AE-3 (10 μM) over the 960 min incubation period, decreasing by 4-fold.

3.5 Naked-eye detection under daylight

Remarkably, the probe exhibited a distinct colorimetric response to Co^{2+} and HClO under daylight, enabling naked eye detection without the need for sophisticated instrumentation. The solution of AE-3 (10 μM) remained colorless upon the addition of the other eleven metal ions (10 μM) besides Co^{2+} but it turned yellow in the presence of Co^{2+} (10 μM) after incubating for 10 min, as observed with the naked eye under daylight (Fig. 13).

At a low concentration, AE-3 (10 μM) was distinctly recognized Co^{2+} by the naked eye under daylight. When Co^{2+} and HClO were separately mixed with the probe and incubated for 10 min, the solution with HClO showed no significant change, while the solution with Co^{2+} turned straw-colored. At higher concentrations (500 μM), naked-eye differentiation between HClO and Co^{2+} was achievable; the solution with HClO turned grass green, while the solution with Co^{2+} turned yellow ochre (Fig. 14).

The development of a functional fluorescent probe capable of identifying specific analytes within environmental contexts is of paramount importance. The application necessitated a thorough investigation into the performance of fluorescent probes within environmental samples. Leveraging probe AE-3's excellent detective ability, to capitalize on the simplicity and timeliness of fluorescent probes, we selected natural water samples from China Pharmaceutical University (CPU), encompassing tap water (T-water), boiled water (B-water), and lake water (L-water). These samples were analyzed without any amendments. As shown in Fig. 15, the probe (10 μM) exhibited a straw-colored transformation in T-water and L-water, whereas B-water remained largely unchanged. This could be attributed to the low concentration of Co^{2+} in B-water, which was insufficient to induce visually perceptible alterations of the solution color. In the case of higher concentrations of the probe solution (100 μM), characteristic color changes indicative of HClO were not observed; the solution color alteration was overshadowed by the straw-colored distinctive of Co^{2+}. This outcome might also stem from the insufficient concentration of HClO in the water to induce a noticeable color change in the probe solution. In summary, the probe exhibited higher sensitivity to Co^{2+} compared to HClO, as evidenced by the probe's lower detection limit.

Fig. 13 Solution of AE-3 (10 μM) with different metal ions (10 μM) in THF/phosphate buffer (1/9, v/v, 50 mM, pH = 7.4) incubated for 10 min and observed in daylight. From left to right, the sequence is: Fe^{3+}, Al^{3+}, Cd^{2+}, Mg^{2+}, Cu^{2+}, Co^{2+}, Ba^{2+}, Ca^{2+}, Cr^{3+}, Mn^{2+}, Ni^{2+}, and Zn^{2+}.

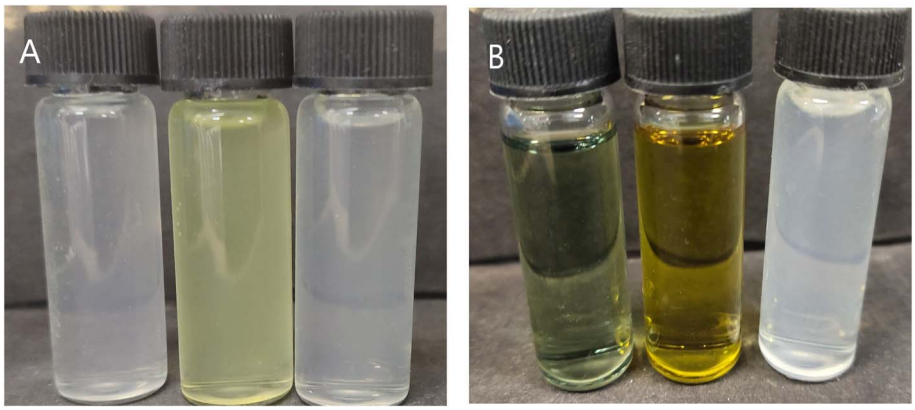

Fig. 14 (A) Solution of AE-3 (10 μM) with HClO and Co^{2+} (10 μM) in THF/phosphate buffer (1/9, v/v, 50 mM, pH = 7.4) incubated for 10 min and observed in daylight. (B) Solution of AE-3 (500 μM) with HClO and Co^{2+} (100 μM) in THF/phosphate buffer (1/4, v/v, 50 mM, pH = 7.4) incubated for 10 min and observed in daylight. From left to right, they are HClO, Co^{2+} and blank samples.

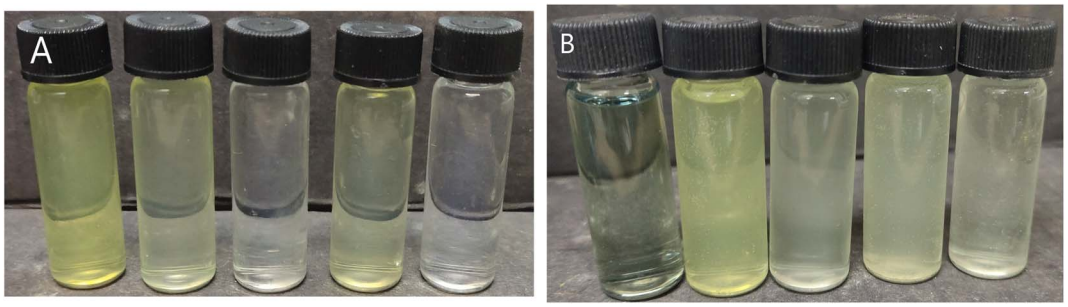

Fig. 15 (A) Mixture of probe AE-3 (10 μM) with Co^{2+} (10 μM) and AE-3 solutions (10 μM) supplemented with various practical water samples, THF/phosphate buffer (1/9, v/v, 50 mM, pH = 7.4). (B) Mixture of probe AE-3 (100 μM) with HClO (500 μM) and AE-3 solutions (100 μM) supplemented with various practical water samples, THF/phosphate buffer (1/4, v/v, 50 mM, pH = 7.4). From left to right, they are the target analyte, T-water, B-water, L-water, and the blank probe samples.

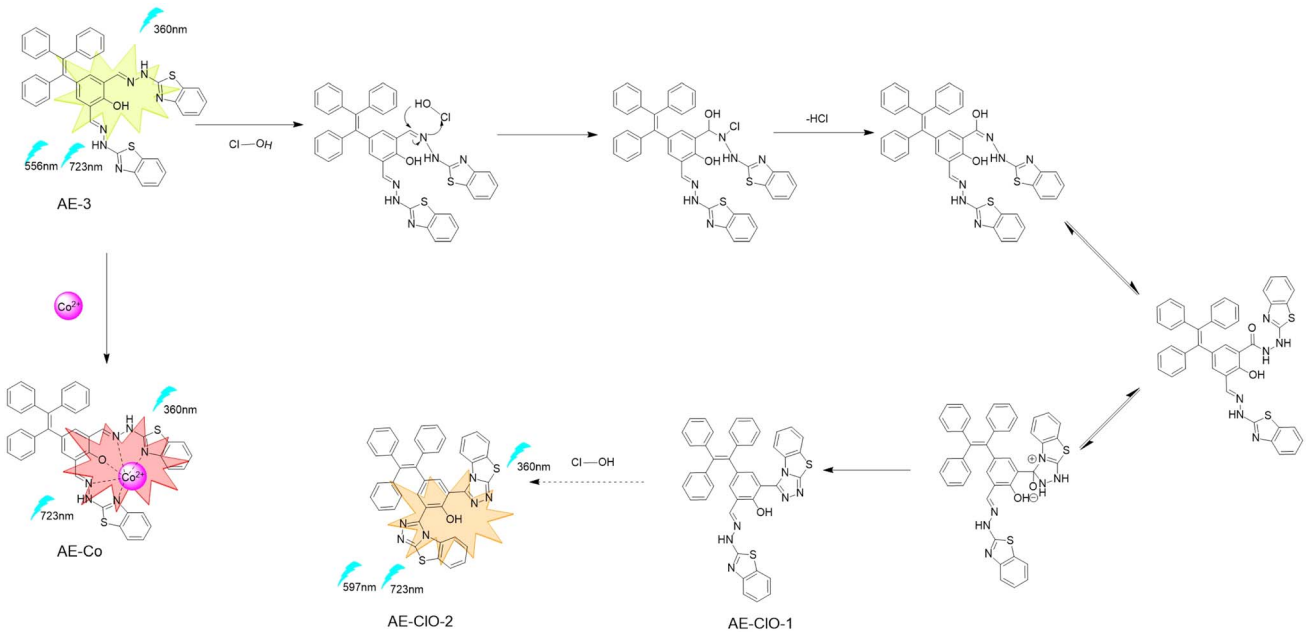

Fig. 16 Recognition mechanism of the probe for HClO and CO^{2+}.

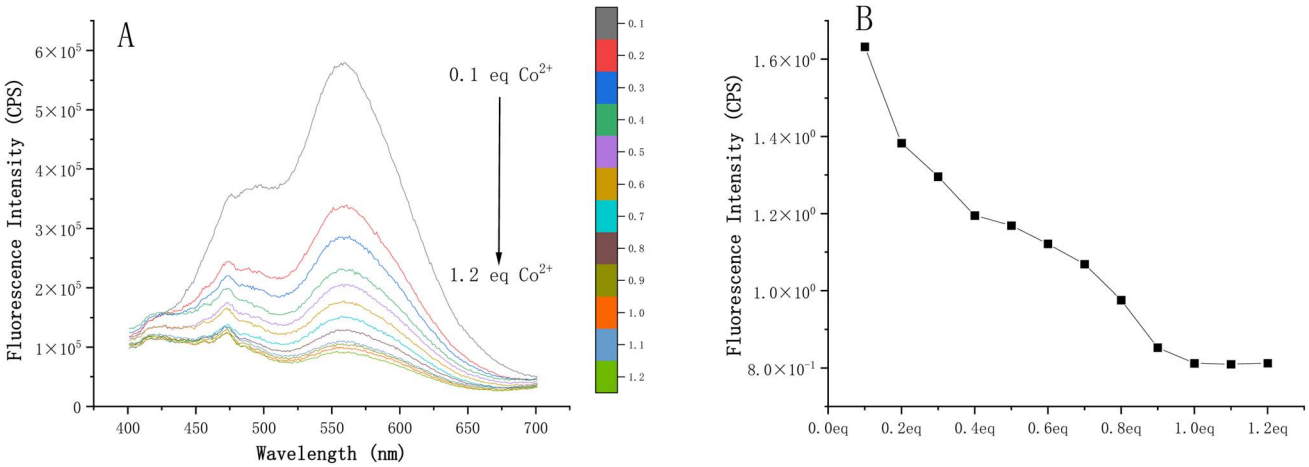

Fig. 17 (A) Fluorescence spectra of AE-3 (10 μM) with the addition of 0.1–1.2 eq. Co^{2+} in THF/phosphate buffer (1/9, v/v, 50 mM, pH = 7.4). (B) Relationship of AE-3 (10 μM) fluorescence intensity at 556 nm and Co^{2+} equivalents in the THF/phosphate buffer (1/9, v/v, 50 mM, pH = 7.4).

3.6 Recognition mechanism study

The proposed identification mechanism is shown in Fig. 16. To further confirm the stoichiometry of AE-3 and Co^{2+}, we performed a continuous titration method. Using the THF/phosphate buffer (1/9, v/v, 50 mM, pH = 7.4) as the solution, a series of gradient volumes of Co^{2+} stock solutions (10 μM) were added to the probe solution (10 μM). We observed that with the increase in Co^{2+} concentration, the fluorescence intensity at 556 nm gradually decreased, eventually reaching a plateau. When the Co^{2+} equivalent reached 1 eq., the fluorescence intensity remained essentially unchanged (Fig. 17). The results showed that the binding stoichiometry between the probe and Co^{2+} was 1 : 1. ESI/MS confirmed this, with a peak at *m*/*z* 756.12 corresponding to $[AE\text{-}3 + Co\text{–}H]^+$, indicating Co^{2+} chelation with the phenolic hydroxyl group and hydrogen atom replacement (Fig. 18). For HClO recognition, after incubating AE-3 with HClO for 12 hours, ESI/MS revealed peaks at *m*/*z* 695.17 ($[AE\text{-}HClO\text{-}1 - H]^-$) and *m*/*z* 693.15 ($[AE\text{-}HClO\text{-}2 - H]^-$), supporting the proposed recognition mechanism (Fig. S17–S21†).

The fluorescence response graphs of the probe to HClO and Co^{2+} further corroborated the recognition mechanism of AE-3. As shown in Fig. 19, HClO quenched the enol-form fluorescence peak at 474 nm and keto-form fluorescence peak at 556 nm, and induced a new fluorescence peak at 597 nm, suggesting that HClO might react with the ESIPT fluorophore of AE-3. Co^{2+}quenched the enol-form and keto-form fluorescence peaks at 474 nm and 556 nm, respectively, likely due to the chelation of Co^{2+} with the probe, which blocked the ESIPT effect.

In the presence of HClO and Co^{2+}, the UV absorption spectrum of the probe exhibited significant changes, which might be related to variations in solubility (Fig. S12†). Upon chelation with Co^{2+}, the probe solubility in polar solvents increased, manifesting as two UV absorption peaks at approximately 221 nm and 206 nm, akin to the benzothiazole structure's original profile. Based on this, the decrease in fluorescence intensity of AE-3 after chelation with Co^{2+} might not only be due to the quenching effect of Co^{2+} but also because the increased solubility reduced the aggregation degree of the probe, thereby

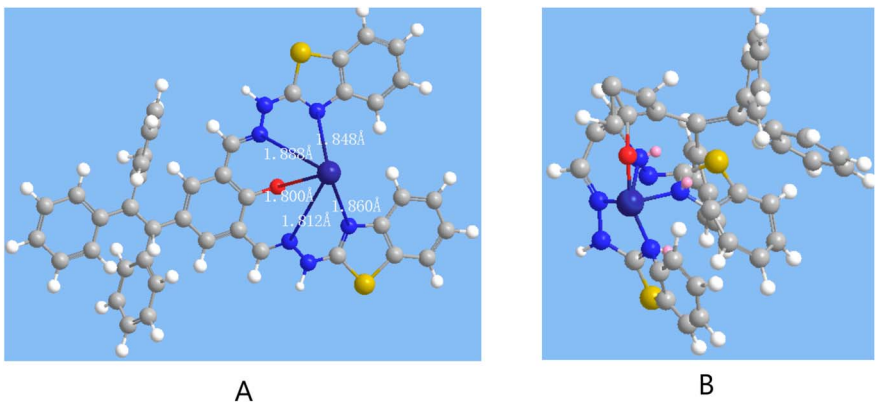

Fig. 18 (A) Bond length of the coordination bond. (B) Chelation of the probe with Co^{2+}.

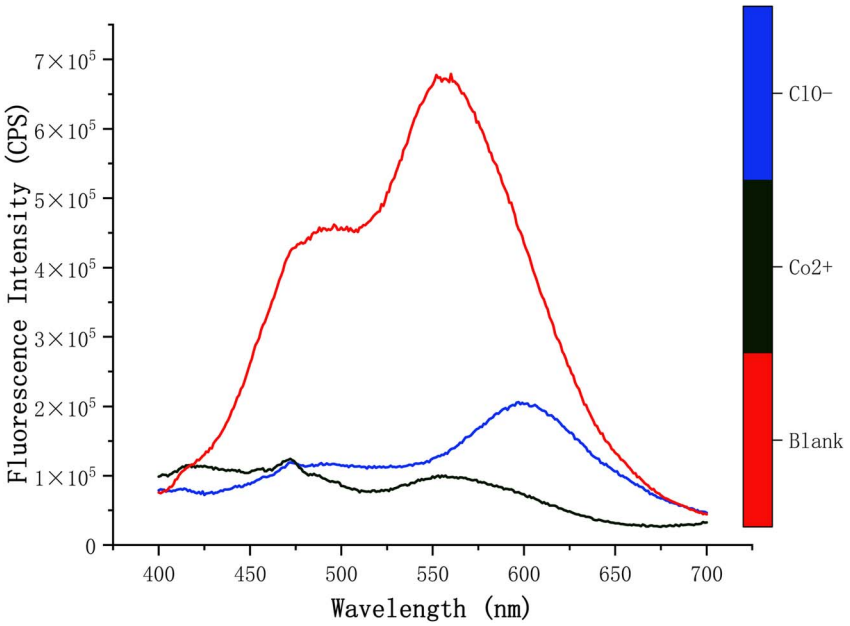

Fig. 19 Fluorescence spectra of AE-3 (10 μM) with the addition of Co^{2+} (10 μM), and HClO (50 μM) in THF/phosphate buffer (1/9, v/v, 50 mM, pH = 7.4).

turning off the AIE effect. Conversely, when the probe was mixed with HClO, a single absorption peak was observed at 206 nm. This change might be attributed to the reaction between the probe and HClO, which disrupted the carbon–nitrogen double bond of the benzothiazole, leading to alterations in the σ–π* transitions. Additionally, the destruction of the Schiff base structure might also contribute to an improvement in the probe's solubility to some extent.

4. Conclusions

In conclusion, we successfully developed a novel fluorescent probe that offers combined ESIPT and AIE effects. This probe exhibited dual-channel fluorescence emission, which indicates its versatile application potential in sensing.

The probe demonstrated high sensitivity and selectivity in detecting Co^{2+} by indicating a change fluorescence intensity at 556 nm. The detection limit for Co^{2+} was 2.823 μM, which was significantly lower than that for HClO, which was 11.55 μM. The association constant of the probe with Co^{2+} was determined to be 475 579.02. Notably, the probe allowed for naked-eye recognition of Co^{2+} under daylight; however, higher concentrations were required for HClO detection with naked eye. The detection of HClO using the probe is interfered with by cobalt ions in practical applications. Overall, this developed probe holds a promising potential for applications in environmental monitoring and water quality detection.

Data availability

The authors confirm that the data supporting the findings of this study are available within the article and/or its ESI.†

Conflicts of interest

There are no conflicts to declare.

Acknowledgements

We are thankful to the National Natural Science Foundation of China for their financial support (No. 21102180).

References

1 S. J. Klebanoff, Myeloperoxidase: friend and foe, *J. Leukocyte Biol.*, 2005, **77**(5), 598–625.
2 C. Liu, Y. Shang, T. Zhao, *et al.*, Facile functionalized fluorescein derivative as a reversible fluorescence probe for selective monitor of the redox cycle between hypochlorous acid and cysteine, *Sens. Actuators, B*, 2021, **348**, 130632.
3 J. C. Genereux, A. K. Boal and J. K. Barton, DNA-Mediated Charge Transport in Redox Sensing and Signaling, *J. Am. Chem. Soc.*, 2010, **132**(3), 891–905.
4 W. Qu, T. Guo, B. Yang, *et al.*, Tracking HOCl by an incredibly simple fluorescent probe with AIE plus ESIPT *in vitro* and *in vivo*, *Spectrochim. Acta, Part A*, 2022, 121649.
5 Y. Yang, Y. Zhao, S. Wei, *et al.*, Colorimetric fluorescence probe detecting Hg2+ and OCl – based on intramolecular charge transfer and excited-state intramolecular proton transfer mechanisms, *J. Lumin.*, 2019, **209**, 102–108.
6 W. A. Prütz, R. Kissner, W. H. Koppenol, *et al.*, On the Irreversible Destruction of Reduced Nicotinamide Nucleotides by Hypohalous Acids, *Arch. Biochem. Biophys.*, 2000, **380**(1), 181–191.

7 P. S. Green, A. J. Mendez, J. S. Jacob, *et al.*, Neuronal expression of myeloperoxidase is increased in Alzheimer's disease, *J. Neurochem.*, 2004, **90**(3), 724–733.
8 Y. W. Yap, M. Whiteman and N. S. Cheung, Chlorinative stress: An under appreciated mediator of neurodegeneration?, *Cell. Signal.*, 2007, **19**(2), 219–228.
9 S. Sugiyama, K. Kugiyama and M. Aikawa, Hypochlorous Acid, a Macrophage Product, Induces Endothelial Apoptosis and Tissue Factor Expression, *Arterioscler., Thromb., Vasc. Biol.*, 2004, **7**(24), 1309–1314.
10 K. C. Huang, C. C. Yang, K. T. Lee, *et al.*, Reduced hemodialysis-induced oxidative stress in end-stage renal disease patients by electrolyzed reduced water, *Kidney Int.*, 2003, **64**(2), 704–714.
11 M. Hausmann, F. Obermeier, D. H. Paper, *et al.*, *In vivo* treatment with the herbal phenylethanoid acteoside ameliorates intestinal inflammation in dextran sulphate sodium-induced colitis, *Clin. Exp. Immunol.*, 2007, **148**(2), 373–381.
12 G. M. Pieper, V. Nilakantan and T. K. Nguyen, Reactive Oxygen and Reactive Nitrogen as Signaling Molecules for Caspase 3 Activation in Acute Cardiac Transplant Rejection, *Antioxid. Redox Signaling*, 2008, **10**, 1031–1039.
13 D. J. Eide, Zinc transporters and the cellular trafficking of zinc, *Biochim. Biophys. Acta Mol. Cell Res.*, 2006, **1763**(7), 711–722.
14 J. González-Montaña, F. Escalera-Valente and A. J. Alonso, Relationship between Vitamin B12 and Cobalt Metabolism in Domestic Ruminant: An Update, *Animals*, 2020, **10**, 1855–1891.
15 X. Wang, W. Zheng, H. Lin, *et al.*, A new selective phenanthroline-based fluorescent chemosensor for Co2+, *Tetrahedron Lett.*, 2009, **50**(14), 1536–1538.
16 S. Goswami, B. Naskar and C. M. Das, A new diformyl phenol based chemosensor selectively detects Zn2+ and Co2+ in the nanomolar range in 100% aqueous medium and HCT live cells, *New J. Chem.*, 2022, 11946–11955.
17 A. Linna, P. Oksa and K. Groundstroem, Exposure to cobalt in the production of cobalt and cobalt compounds and its effect on the heart, *Occup. Environ. Med.*, 2004, **61**(11), 877–885.
18 D. Maity, A. Raj, D. Karthigeyan, *et al.*, Reaction-based probes for Co(ii) and Cu(i) with dual output modes: fluorescence live cell imaging, *RSC Adv.*, 2013, **3**(37), 16788–16794.
19 A. R. Khorrami, T. Hashempur, A. Mahmoudi, *et al.*, Determination of ultra trace amounts of cobalt and nickel in water samples by inductively coupled plasma-optical emission spectrometry after preconcentration on modified C18-silica extraction disks, *Microchem. J.*, 2006, **84**, 75–79.
20 Y. Saini, K. K. Greenwood, C. Merrill, *et al.*, Acute Cobalt-Induced Lung Injury and the Role of Hypoxia-Inducible Factor 1α in Modulating Inflammation, *Toxicol. Sci.*, 2010, **116**(2), 673–681.
21 O. Karovic, I. Tonazzini, N. Rebola, *et al.*, Toxic effects of cobalt in primary cultures of mouse astrocytes, *Biochem. Pharmacol.*, 2007, **73**(5), 694–708.
22 N. O. Soto, B. Horstkotte, J. G. March, *et al.*, An environmental friendly method for the automatic determination of hypochlorite in commercial products using multisyringe flow injection analysis, *Anal. Chim. Acta*, 2008, **611**(2), 182–186.
23 A. P. Soldatkin, D. V. Gorchkov, C. Martelet, *et al.*, New enzyme potentiometric sensor for hypochlorite species detection, *Sens. Actuators, B*, 1997, **43**(1–3), 99–104.
24 T. M. Jeitner, H. Xu and G. E. Gibson, Inhibition of the a-ketoglutarate dehydrogenase complex by the myeloperoxidase products, hypochlorous acid and mono-N-chloramine, *J. Neurochem.*, 2005, **92**, 302–310.
25 M. Shahbaz, B. Dar, S. Sharif, *et al.*, Recent advances in the fluorimetric and colorimetric detection of cobalt ions, *RSC Adv.*, 2024, **14**(14), 9819–9847.
26 P. Xing, Z. Zhang, Y. Niu, *et al.*, Water solubility is essential for fluorescent probes to image hypochlorous acid in live cells, *Chem. Commun.*, 2018, **54**(71), 9889–9892.
27 D. Shi, S. Chen and B. Dong, Evaluation of HOCl-generating anticancer agents by an ultrasensitive dual-mode fluorescent probe, *Chem. Sci.*, 2019, **10**(13), 3715–3722.
28 L. Yuan, L. Wang, B. K. Agrawalla, *et al.*, Development of Targetable Two-Photon Fluorescent Probes to Image Hypochlorous Acid in Mitochondria and Lysosome in Live Cell and Inflamed Mouse Model, *J. Am. Chem. Soc.*, 2015, **137**(18), 5930–5938.
29 Y. Yang, Q. Zhao, W. Feng, *et al.*, Luminescent Chemodosimeters for Bioimaging, *Chem. Rev.*, 2013, **113**(1), 192–270.
30 W. Xu, Z. Zeng, J. H. Jiang, *et al.*, Discerning the Chemistry in Individual Organelles with Small-Molecule Fluorescent Probes, *Angew. Chem., Int. Ed.*, 2016, **55**(44), 13658–13699.
31 X. Chen, X. Tian, I. Shin, *et al.*, Fluorescent and luminescent probes for detection of reactive oxygen and nitrogen species, *Chem. Soc. Rev.*, 2011, **40**(9), 4783–4804.
32 X. Li, X. Gao, W. Shi, *et al.*, Design Strategies for Water-Soluble Small Molecular Chromogenic and Fluorogenic Probes, *Chem. Rev.*, 2014, **114**(1), 590–659.
33 W. Sun, S. Guo, C. Hu, *et al.*, Recent Development of Chemosensors Based on Cyanine Platforms, *Chem. Rev.*, 2016, **116**(14), 7768–7817.
34 Z. Xu, J. Chen, L. L. Hu, *et al.*, Recent advances in formaldehyde-responsive fluorescent probes, *Chin. Chem. Lett.*, 2017, **28**(10), 1935–1942.
35 J. Chan, S. C. Dodani and C. J. Chang, Reaction-based small-molecule fluorescent probes for chemoselective bioimaging, *Nat. Chem.*, 2012, **4**(12), 973–984.
36 D. Wu, Y. Shen, J. Chen, *et al.*, Naphthalimide-modified near-infrared cyanine dye with a large stokes shift and its application in bioimaging, *Chin. Chem. Lett.*, 2017, **28**(10), 1979–1982.
37 S. Ghazali, J. Wang, J. Fan, *et al.*, Selective imaging of Co2+ in live cells with a "turn-on" fluorescent probe, *Sens. Actuators, B*, 2017, **239**, 1237–1242.
38 D. Kim, A. Jo, B. K. Seo, *et al.*, Colorimetric Detection of Transition Metal Ions with Azopyridine-based Probing Molecule in Aqueous Solution and in PMMA Film.

39 L. Shi, S. Yang and H. J. Hong, A novel target and pH dual-activatable fluorescent probe for precisely detecting hypochlorite in lysosomes, *Anal. Chim. Acta*, 2020, **1094**, 122–129.

40 Q. Xia, X. Wang and Y. Liu, An endoplasmic reticulum-targeted two-photon fluorescent probe for bioimaging of HClO generated during sleep deprivation, *Spectrochim. Acta, Part A*, 2020, **229**, 117992.

41 Z. Zhu, H. Ding, Y. Wang, *et al.*, Rational design of a FRET-based ratiometric fluorescent chemosensor for detecting ClO− with large Stokes based on rhodamine and naphthalimide fluorophores, *Tetrahedron*, 2020, **76**(26), 131291.

42 C. Xu and Y. Qian, The α, β-unsaturated pyrazolone-based fluorescent sensor with red emission and its application for real-time monitoring hypochlorite in cancer cells and zebrafish, *Dyes Pigm.*, 2019, **161**, 303–312.

43 J. Yang, A near-infrared fluorescent probe based on phosphorus-substituted rhodamine for deep imaging of endogenous hypochlorous acid in vivo, *Sens. Actuators, B*, 2020, **307**, 127652.

44 L. Chen, S. J. Park, D. Wu, *et al.*, A two-photon ESIPT based fluorescence probe for specific detection of hypochlorite, *Dyes Pigm.*, 2018, **158**, 526–532.

45 L. Wu, Q. Yang, L. Liu, *et al.*, ESIPT-based fluorescence probe for the rapid detection of hypochlorite (HOCl/ClO^-), *Chem. Commun.*, 2018, **54**(61), 8522–8525.

46 A. Weller, Über die Fluoreszenz der Salizylsäure und verwandter Verbindungen, *Naturwissenschaften*, 1955, **42**(7), 175–176.

47 H. Ren, F. Huo, X. Wu, *et al.*, An ESIPT-induced NIR fluorescent probe to visualize mitochondrial sulfur dioxide during oxidative stress in vivo, *Chem. Commun.*, 2020, **57**, 655–657.

48 A. Bi, M. Liu, S. Huang, *et al.*, Construction and theoretical insights into the ESIPT fluorescent probe for imaging formaldehyde *in vitro* and *in vivo*, *Chem. Commun.*, 2021, **57**(28), 3496–3499.

49 H. C. Zhang, D. H. Tian, Y. L. Zheng, *et al.*, Designing an ESIPT-based fluorescent probe for imaging of hydrogen peroxide during the ferroptosis process, *Spectrochim. Acta, Part A*, 2021, **248**, 119264.

50 C. Wu, H. Xu, Y. Li, *et al.*, An ESIPT-based fluorescent probe for the detection of phosgene in the solution and gas phases, *Talanta*, 2019, **200**, 78–83.

51 Y. Li, D. Dahal, C. S. Abeywickrama, *et al.*, Progress in Tuning Emission of the Excited-State Intramolecular Proton Transfer (ESIPT)-Based Fluorescent Probes, *ACS Omega*, 2021, **6**(10), 6547–6553.

52 V. V. Shynkar, A. S. Klymchenko, C. Kunzelmann, *et al.*, Fluorescent Biomembrane Probe for Ratiometric Detection of Apoptosis, *J. Am. Chem. Soc.*, 2007, **129**(7), 2187–2193.

53 Y. Zhang, Y. Deng, N. Ji, *et al.*, A rationally designed flavone-based ESIPT fluorescent chemodosimeter for highly selective recognition towards fluoride and its application in live-cell imaging, *Dyes Pigm.*, 2019, **166**, 473–479.

54 N. N. Mohd Yusof Chan, A. Idris, Z. H. Zainal Abidin, *et al.*, White light employing luminescent engineered large (mega) Stokes shift molecules: a review, *RSC Adv.*, 2021, **11**(22), 13409–13445.

55 V. S. Padalkar and S. Seki, Excited-state intramolecular proton-transfer (ESIPT)-inspired solid state emitters, *Chem. Soc. Rev.*, 2016, **45**(1), 169–202.

56 C. Lu, J. Xu, Z. Song, *et al.*, Advancements in ESIPT probe research over the past three years based on different fluorophores, *Dyes Pigm.*, 2024, **224**, 111994.

57 J. Luo, Z. Xie and J. W. Y. Lam, Aggregation-induced emission of 1-methyl-1,2,3,4,5-pentaphenylsilole, *Chem. Commun.*, 2001, 1740–1741.

58 K. Wang, D. Xi, C. Liu, *et al.*, A ratiometric benzothiazole-based fluorescence probe for selectively recognizing HClO and its practical applications, *Chin. Chem. Lett.*, 2020, **31**(11), 2955–2959.